JOURNAL OF GEOPHYSICAL RESEARCH, VOL. 114, A05301, doi:10.1029/2008JA013765, 2009

Joule heating and nitric oxide in the thermosphere

C. A. Barth,[1] G. Lu,[2] and R. G. Roble[2]

Received 24 September 2008; revised 21 January 2009; accepted 29 January 2009; published 7 May 2009.

[1] The effect of Joule heating on the density of nitric oxide in the thermosphere was studied using observations from the Student Nitric Oxide Explorer (SNOE) satellite and model calculations from the Thermospheric Ionosphere Electrodynamics General Circulation Model for a Joule heating event that occurred on 25 September 1998. Model results and SNOE observations from fifteen orbits were compared in the latitude range 82°S to 82°N over the altitude range 100–150 km. Joule heating which occurred in the 55°- to 60°-latitude region produced a meridional wind blowing equatorward and a gravity wave propagating equatorward, which caused an increase in the temperature of the thermosphere in the 20°- to 75°-latitude region. When the heated thermosphere was illuminated by solar radiation, the density of nitric oxide increased over this entire latitude region because of a temperature-sensitive reaction between ground state nitrogen atoms and molecular oxygen. In the 24 hours following the Joule heating event, the increased nitric oxide diffused downward from the 150-km region to the 110-km level of the thermosphere.

Citation: Barth, C. A., G. Lu, and R. G. Roble (2009), Joule heating and nitric oxide in the thermosphere, *J. Geophys. Res.*, *114*, A05301, doi:10.1029/2008JA013765.

1. Introduction

[2] The density of thermospheric nitric oxide in the auroral region increases during geomagnetic storms as a result of electron precipitation and Joule heating. This paper deals with the effect of Joule heating on the nitric density using observations from the Student Nitric Oxide Explorer (SNOE) satellite and the National Center for Atmospheric Research Thermospheric Ionosphere Electrodynamics General Circulation Model (NCAR TIEGCM). This problem has been studied earlier using observations from the Solar Mesosphere Explorer satellite (SME) and the National Center for Atmospheric Research Thermosphere General Circulation Model (NCAR TGCM) [*Siskind et al.*, 1989]. Since the SNOE nitric oxide observations have fifteen orbits a day as contrasted with the SME observations of only two orbits a day, it is possible to study the temporal variations of the thermosphere in more detail. The TIEGCM [*Roble et al.*, 1998; *Richmond et al.*, 1992] has evolved from the TGCM [*Roble and Ridley*, 1987] to now include a calculation of ionospheric and electrodynamic processes. In addition, the ionospheric convection and auroral precipitation parameters are derived using the AMIE (Assimilative Mapping of Ionospheric Electrodynamics) procedure [*Richmond and Kamide*, 1988].

[3] Electron precipitation produces nitric oxide in the thermosphere through its ionization and dissociation of molecular nitrogen and the subsequent reaction of excited nitrogen atoms with molecular oxygen. The maximum density of nitric oxide produced by electron precipitation occurs near 110 km at geomagnetic latitudes in the 60°–70° region [*Barth et al.*, 2003]. Above 110 km the altitude dependence follows the density distribution of molecular nitrogen and molecular oxygen. There is a seasonal variation in the nitric oxide density produced by electron precipitation with greater amounts during the winter and a minimum at the summer solstice [*Barth and Bailey*, 2004; *Barth et al.*, 2004].

[4] The earlier study by *Siskind et al.* [1989] clearly showed that the nitric oxide density increases as a result of the temperature increase during the Joule heating event owing to the role played by the temperature-sensitive reaction between ground-state nitrogen atoms and molecular oxygen. Their study also showed that Joule heating in the auroral region caused an increase in thermospheric temperatures at midlatitudes and that the increased nitric oxide at midlatitudes diffused downward. *Richards* [2004] in examining nitric oxide observations made from the Atmosphere Explorer (AE-C) satellite has also suggested that downward transport plays a role in increasing nitric oxide at lower altitudes during geomagnetic storms. *Dobbin and Aylward* [2008] have used a global circulation model simulation to show how it is possible for meridional winds to transport nitric oxide equatorward at high altitudes followed by downward transport to increase low-altitude nitric oxide at mid latitudes during a magnetic storm.

[5] This study focuses on the role of winds and gravity waves on the temperature and on the photochemistry of nitric oxide during and following the Joule heating event. Outstanding questions are: Is the increase of nitric oxide density equatorward of the auroral region the result of the

[1]Laboratory for Atmospheric and Space Physics, University of Colorado, Boulder, Colorado, USA.
[2]High Altitude Observatory, National Center for Atmospheric Research, Boulder, Colorado, USA.

0148-0227/09/2008JA013765$09.00

Table 1. Longitude and Universal Time (UT) at Latitude 40°N for the Fifteen Orbits on Day 268

Orbit	Longitude (°E)	UT (Hours)
1	143	0.5
2	119	2.1
3	95	3.7
4	71	5.3
5	47	6.9
6	23	8.5
7	359	10.1
8	335	11.6
9	311	13.2
10	287	14.8
11	263	16.4
12	239	18.0
13	215	19.6
14	191	21.2
15	167	22.8

transport of nitric oxide molecules or the transport of heat from the auroral region toward the equator? Is there observational evidence for the downward flow of nitric oxide at midlatitudes leading to an increase in the nitric oxide density at 110 km?

[6] The Joule heating event chosen for this study occurred at 0600 UTC on 25 September 1998 (day of the year 268). Increased geomagnetic activity started the previous day at about 1800 hours with increased auroral electron precipitation. The Joule heating rate was at a maximum at 0400 hours and 0600 hours on day 268. The model was run for the three day period 267–269.

2. SNOE Observations

[7] Global observations of nitric oxide were made from the limb scanning ultraviolet spectrometer on the SNOE spacecraft [*Barth et al.*, 2003]. The sun-synchronous orbit provided coverage from 82 S to 82 N on 15 orbits a day spaced 24 degrees apart in longitude at a local time of 1100 hours. The data set from the primary mission extends from March 1998 to September 2000. The density of nitric oxide was determined by measuring the fluorescent scattering of solar radiation at 237 nm in the (0,1) gamma band. A g factor of 2.62×10^{-6} photons/s molecule was used [*Stevens*, 1995]. The limb scanning instrument covered the altitude range 100–150 km at a resolution of 3.3 km. The latitude resolution in the data set was 5 degrees. The SNOE data used in this study is taken from the SNOE database, version 2, channel 2 (see nssdc.gsfc.nasa.gov).

3. TIEGCM

[8] The TIEGCM is a three dimensional thermospheric global circulation model that calculates the neutral winds, the temperature, and the mixing ratios of N_2, O_2, O, $N(^2D)$, $N(^4S)$, and NO at a resolution of 5° latitude and 5° longitude at 29 pressure levels between 97 km and 500 km [*Roble et al.*, 1988; *Richmond et al.*, 1992].This model calculates the neutral and ion densities and electric fields and currents in a self-consistent scheme [*Roble and Ridley*, 1994]. The model is described in detail on the HAO web site with a description of the equations and the overall structure [www.hao.ucar.edu/modeling/tgcm/].

4. AMIE Procedure

[9] The AMIE procedure provides global maps of ionospheric electrodynamic fields through least squares fit of various space and ground based data sets. For this particular event, the data inputs to AMIE include auroral particle measurements from 4 DMSP satellites (F11–F14) and 2 NOAA satellites (NOAA-12 and NOAA-14), ion drifts from the DMSP satellites and from 6 SuperDARN radars located in the northern hemisphere, along with magnetic perturbations recorded at 131 worldwide magnetometer stations. Global patterns of ionospheric convection and auroral energy flux and mean energy are derived in both northern and southern hemispheres at a 5-min cadence. The AMIE patterns are then timely interpolated and imposed as the upper boundary inputs to the TIEGCM, which ran at a time step of 2 minutes [see *Lu et al.*, 1995, 2001] for more details on the coupled AMIE-TIEGCM).

5. Model Results and Discussion

[10] For the discussion of the model results, we have chosen an altitude of 150 km. This is the highest altitude where the SNOE observations have a satisfactory signal to noise ratio. Joule heating started at 0400 hours on day 268. It reached a peak at 0600 hours and decreased in intensity until 1000 hours. The Joule heating extended from longitude 239°E to 359°E at latitude 55°N and from longitude 191°E to 47°E at latitude 60°N. Joule heating did not extend equatorward of 55°N and S.

[11] The plan of this analysis is to first examine the model results at a single longitude at all latitudes as a function of time before and after the Joule heating event to determine the processes that produce an increase in nitric oxide densities at midlatitudes. Then we compare the model calculations to the SNOE observations of nitric oxide density which were made during fifteen orbits a day. These orbits followed fifteen different longitude tracks at orbit inclination of 97°. The solar local time was constant while the universal time increased by 1.6 hours between adjacent orbits. Table 1 shows the longitude and universal time of the fifteen orbits on day 268 at a latitude of 40°N.

[12] For the study of the model results as a function of time, we have chosen the longitude region where the maximum Joule heating occurred. At a longitude of 335°E and latitude of 60°N, the temperature at 150 km increased to over 1000°K from its quiet time value of less than 700 K.

5.1. As Function of Time

[13] Some of the results of the model calculations are shown in Figure 1 as a function of time for the days 267, 268, and 269. The Joule heating event took place on day 268.

[14] Figure 1 (top) shows the nitric oxide density as a function of time for the three day period at a latitude of 60°N. It reaches a maximum at 1300 hours on day 268 which is noon solar local time. Earlier the nitric oxide increased during the night as a result of electron precipita-

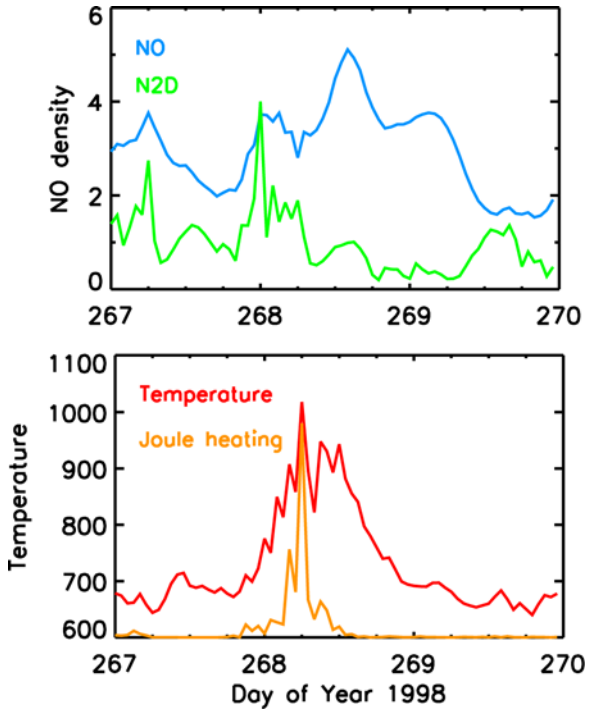

Figure 1. TIEGCM results at 150 km at 60°N, 335°E as function of time on days 267, 268, and 269. (top) NO density (10^7 molecules/cm^3) (blue). Maximum occurs at 1300 hours on day 268. N(^{2}D) density (arbitrary units) (green) used as an indicator of electron precipitation. Maximum at 0000 hours on day 268. (bottom) Temperature (C°) (red). Maximum at 0600 hours on day 268. Joule heating (arbitrary units) (orange). Maximum also occurs at 0600 hours on day 268.

tion. The occurrence of electron precipitation is indicated by the variation in the N(^{2}D) density which is also plotted in Figure 1. Enhanced electron precipitation took place between 2100 hours on day 267 and 0600 hours on day 268. As a result, the NO density also increases during this time.

[15] At 0400 hours and 0600 hours on day 268, there is a strong Joule heating event at 60°N (Figure 1, bottom). The temperature reaches a maximum at 0600 hours and then gradually cools during the following 24 hours (Figure 1, bottom). The NO density increases starting at sunrise at 0700 hours and peaks at local noon and then decreases to its previous value at 1900 hours (Figure 1, top).

[16] Figure 1 (top) clearly shows that the nitric oxide density increases following the Joule heating intensification at 0600 hours on day 268. However, the maximum in the nitric oxide density occurs at 1300 hours which is noon local solar time. The temperature increase occurs earlier, but the atmosphere needs to be illuminated by solar radiation for the nitric oxide density to increase as a result of the temperature increase.

5.2. As Function of Latitude

[17] The behavior of NO based on the TIEGCM simulations is plotted in Figures 2a–2c as a function of latitude. The time period when electron precipitation, 0000 hours to 0600 hours on day 268, was in control of the density of NO is shown in Figure 2a. The time interval when Joule heating was controlling the NO density, 0700 hours to 1300 hours, is shown in Figure 2b. Figure 2c contains the recovery period from 1400 hours to 2000 hours when the temperature is returning to normal and the winds have quieted down.

[18] In Figure 2a, NO is plotted as a function of latitude (0°N–80°N) for each hour between 0 and 6 hours. This shows the movement of NO from 60°N–70°N toward the equator at the rate of about 4 degrees per hour (120 m/s). This is the signature of winds blowing the NO equatorward.

[19] Figure 2b shows the behavior of NO from sunrise until local noon following the period of Joule heating. This shows the result of the increase in temperature moving rapidly equatorward followed by the action of the increasing solar radiation on the heated atmosphere. The NO density increases at all latitudes as the solar elevation angle increases. This is the signature of Joule heating causing the NO to increase at midlatitudes.

[20] Figure 2c shows the behavior of NO during the period when the temperature of the atmosphere is decreasing and the intensity of the solar radiation is also decreasing. The NO density decreases at all latitudes.

[21] The behavior of the temperature during the electron precipitation event is shown in Figure 2d. Figure 2d shows that during electron precipitation the temperature increases near 70°N. At the end of this six hour period, the increased temperature extends equatorward to 55°N. The temperature increase has moved 15° of latitude in six hours at a velocity of 77 m/s.

[22] Figure 2e shows the dramatic temperature changes following the Joule heating event. At 0700 hours, there is a large increase in temperature with a maximum at 70°N. There is a secondary maximum at 35°N. The temperature increase has propagated equatorward very rapidly. At 0600 hours the temperature maximum was at 60°N and at 0700 hours there was a temperature maximum at 35°N. The increase in temperature propagated equatorward 25° of latitude in one hour at a velocity of 770 m/s. The temperature behavior at 0800 hours is similar with a maximum at 70°N and a secondary maximum at 30°N. At 0900 hours the temperature maximum is at 60°N and at 10 hours it has moved to 55°N. During the remaining period the temperature decreases at all latitudes as shown in Figure 2f.

[23] The behavior of the winds during the electron precipitation period is shown in Figure 3a and of the Joule heating period in Figure 3b. In Figure 3a, there is a strong southward meridional wind between 60°N and 80°N from 0000 hours until 0500 hours followed by a continuous southward wind at all latitudes equatorward of 55°N from 0100 hour until 0600 hours.

[24] Figure 3b shows the strong southward meridional wind at 0700 hours immediately following the Joule heating event at 0600 hours. The maximum southward wind velocity is 300 m/s at 0700 hours. There is a strong southward wind between 20°N and 60°N between 0700 to 0800 hours. During the period 0900–1300 hours, the winds decrease equatorward of 55°N.

[25] The behavior of the vertical wind is shown in Figures 3c and 3d. At 60°N, there is an upward flow of 10 m/s at 0400 hours dropping to 8 m/s at 0600 hours. Following this period, the vertical winds are quiet. These

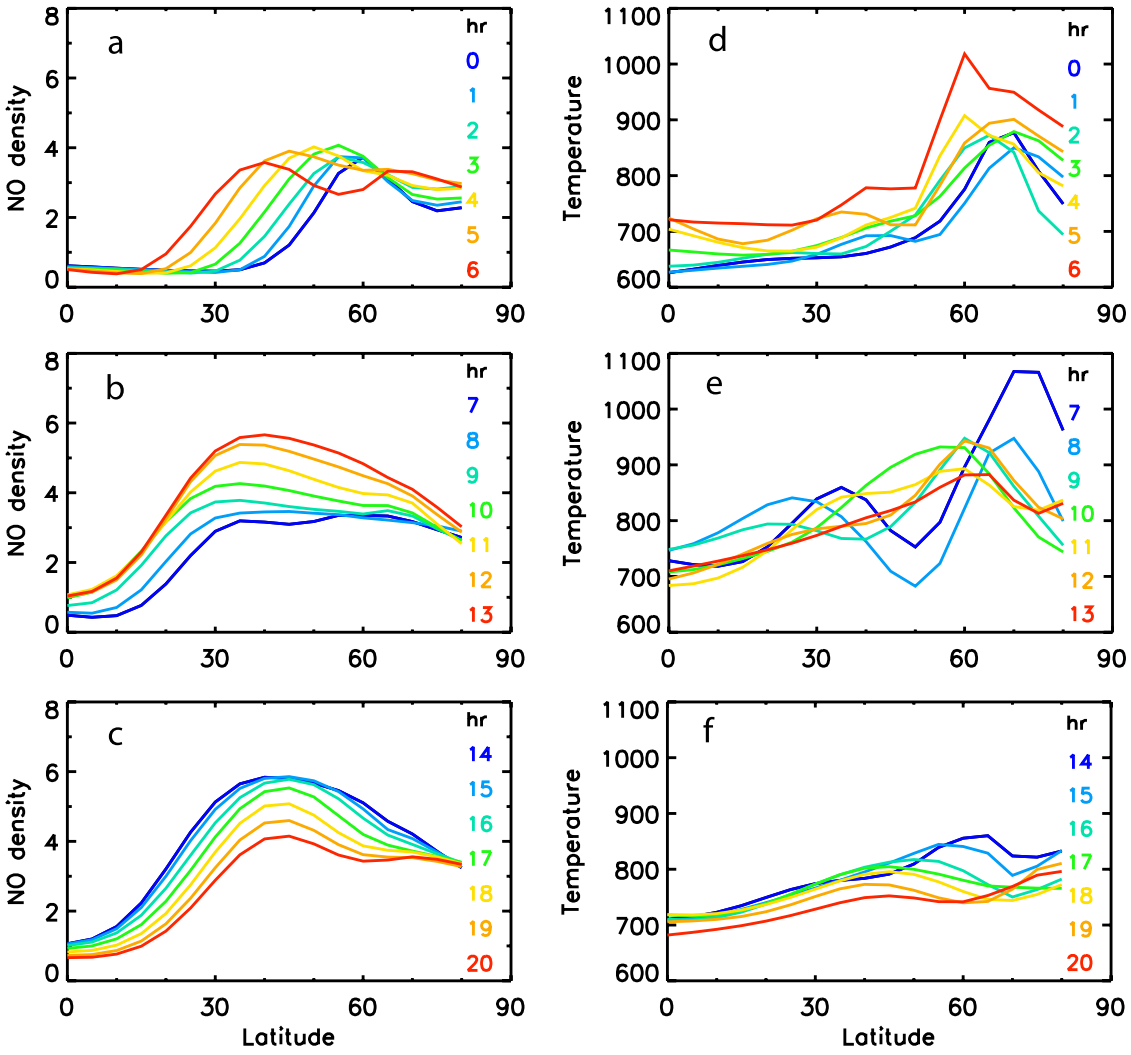

Figure 2. TIEGCM results at 150 km at 335°E as a function of latitude and time on day 268. (a) NO density (10^7 molecules/cm^3) for 7 hours, starting at 0000 hours (violet) to 0600 hours (red). NO moves equatorward. (b) NO density from 0700 hours (violet) to 1300 hours (red). NO increases at all latitudes. (c) NO density from 1400 hours (violet) to 2000 hours (red). NO decreases at all latitudes. (d) Temperature (°C) for 7 hours, starting at 0000 hours (violet) to 0600 hours (red). Temperature increases in latitude region 60°N–70°N. (e) Temperature from 0700 hours (violet) to 1300 hours (red). Temperature wave moves equatorward. (f) Temperature from 1400 hours (violet) to 2000 hours (red). Temperature decreases at all latitudes.

winds produce upwelling of molecular oxygen during the electron precipitation and Joule heating events.

5.3. As Function of Longitude

[26] The behavior of NO and the winds from the TIEGCM calculations were plotted as a function of latitude for the remaining fourteen longitudes and times listed in Table 1 in the same format as was done for longitude 335°E in Figure 2. For longitudes 143°, 119°, 95°, and 71° (orbits 1–4), the behavior of the winds and the NO density distribution was normal with both showing increases north of 60°N latitude. For longitudes that were sampled after the Joule heating event at 0600 hours, longitudes 47°, 23°, 359°, 335°, 311°, 287°, 263°, 239°, 215°, and 191° the temperature showed a pressure wave propagating equatorward causing increased NO densities at midlatitudes following the same pattern that is shown in Figure 2. For a longitude where the Joule heating event did not take place, longitude 167°, the winds and increased nitric oxide were confined to the polar region north of 60°N.

6. Photochemical Reactions

[27] During the electron precipitation event at 60°N, the impacting electrons cause ionization and dissociation of molecular nitrogen. When the sun is illuminating the thermosphere, photoelectrons produced from the action of solar soft X rays also cause ionization and dissociation of molecular nitrogen. Both process lead to the production of excited nitrogen atoms in the N(^{2}D) state (2.38 eV). The excited

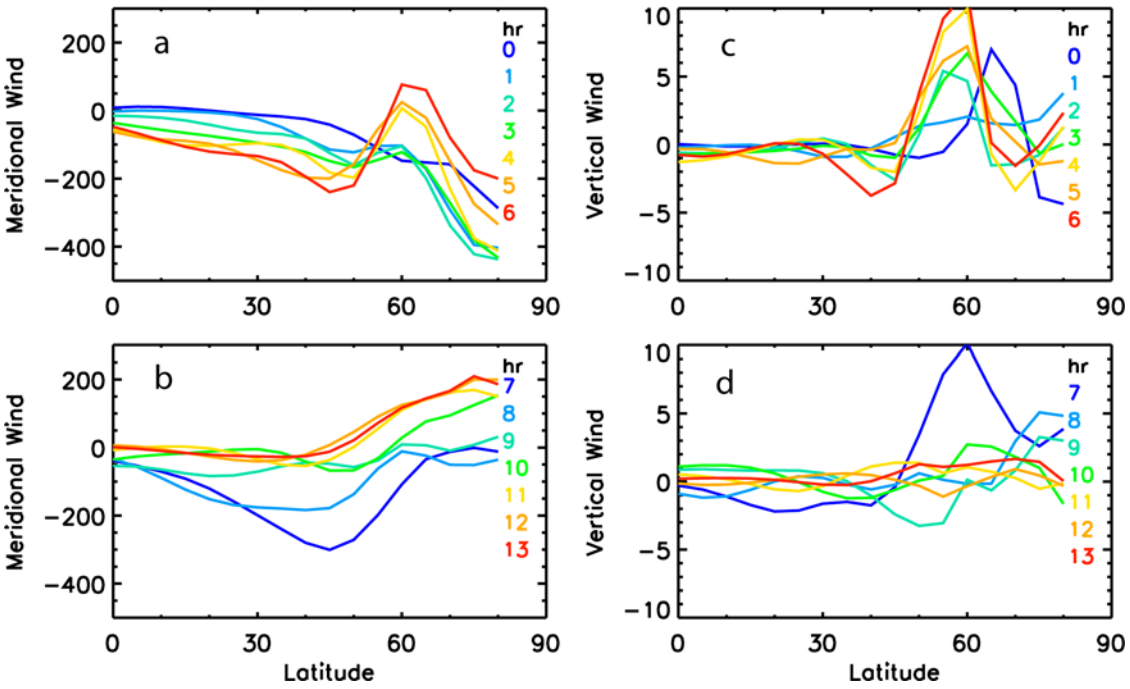

Figure 3. TIEGCM results at 150 km at 335°E as a function of latitude and time on day 268. (a) Meridional wind (m/s) for 7 hours from 0000 hours (violet) until 0600 hours (red). There is a large southward wind at 75°N. (b) Meridional wind from 0700 hours (violet) until 1300 hours (red). There is a large southward wind at 45°N. (c) Vertical wind (m/s) from 0000 hours (violet) until 0600 hours (red). There is strong upwelling at 0500–0600 hours. (d) Vertical wind from 0700 hours (violet) until 1300 hours (red). Strong upwelling continues at 7000 hours.

nitrogen atoms react rapidly with molecular oxygen to produce nitric oxide.

$$N(^2D) + O_2 \rightarrow NO + O. \qquad 5.0 \times 10^{-12}\ cm^3s^{-1} \qquad (1)$$

[28] This is the principal reaction that produces NO in the thermosphere. The reaction rate coefficients that are listed are those that are used in the TIEGCM (see HAO Web site).

[29] The principal reaction that destroys NO is its reaction with ground state nitrogen atoms $N(^4S)$.

$$N(^4S) + NO \rightarrow N_2 + O.\ 1.6 \times 10^{-10}\ \exp(-460/T)\ cm^3s^{-1} \quad (2)$$

[30] The ground state nitrogen atoms are also produced from various reactions initiated by the precipitating electrons. When the sun is illuminating the atmosphere, it is the photoelectrons produced from the action of solar soft X rays on the atmospheric constituents that lead to the production of $N(^2D)$ and $N(^4S)$ atoms.

[31] The $N(^4S)$ atoms also react with molecular oxygen in a temperature-dependent reaction.

$$N(^4S) + O_2 \rightarrow NO + O.\ \ 1.5 \times 10^{-11}\exp(-3600/T)\ cm^3s^{-1} \ (3)$$

[32] This reaction makes a contribution to the production of NO, but the $N(^2D)$ reaction is usually the principal source of NO. The $N(^4S)$ reaction with molecular oxygen is also a loss mechanism for the $N(^4S)$ atoms, but its reaction with NO is usually the dominant loss mechanism.

[33] Using these reactions, we can describe the behavior of NO during the electron precipitation and Joule heating events. The ionization and dissociation of molecular nitrogen that is produced by electron impact leads to the production of larger amounts of $N(^2D)$ atoms than $N(^4S)$ atoms principally because the branching ratio of the dissociative recombination of ionized nitric oxide favors the $N(^2D)$ state by a ratio of 6:1. Thus electron impact events directly produce an increase in the density of nitric oxide at 60°N as is shown in Figure 1a.

[34] The loss of nitric oxide is controlled by the photodissociation of nitric oxide.

$$NO + h\nu \rightarrow N(^4S) + O. \qquad 4.5 \times 10^{-6}\ s^{-1} \qquad (4)$$

[35] The effective lifetime of the loss of nitric oxide that is illuminated by the sun is 19.6 hours. Because of this long photochemical lifetime, meridional winds are able to blow nitric oxide equatorward as is shown in Figure 2a.

[36] The processes that lead to an increase in the density of nitric oxide following a Joule heating event are quite different. The Joule heating event occurred at 0400 hours and 0600 hours at 60°N (Figure 1, bottom). The temperature reached a peak at 0600 hours and then slowly cooled during the following 18 hours. The NO density did not start to increase until 0700 hours when the atmosphere was illuminated by the sun and the NO density reach a maximum just past local noon (Figure 1, top).

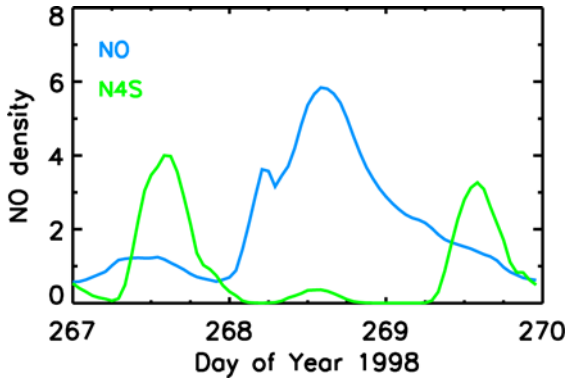

Figure 4. TIEGCM results at 150 km at 40°N, 335°E as function of time on days 267, 268, and 269. NO density (10^7 molecules/cm^3 (blue). Maximum occurs at 1300 hours on day 268. N(^{4}S) density (arbitrary units) (green). N(^{4}S) decreases on day 268 as compared to days 267 and 269.

[37] At 40°N the temperature increased quickly reaching a maximum at 0700 hours (Figure 2e). The NO density increased starting at 0700 hours (local sunrise) and reached a maximum at 1300 hours UT which was 1200 hours solar local time. With the sun illuminating the atmosphere, N(^{2}D) and N(^{4}S) atoms were produced resulting in the production of NO. With the higher temperatures, reaction 3 caused an increase in the loss rate of N(^{4}S) atoms. With less N(^{4}S) the NO increased because the loss rate of NO decreased (reaction 2). A maximum in the NO density is reached at 1300 hours (local noon) (Figure 2b) and then there is a gradual decrease controlled by the decreasing temperature and the photodissociation reaction 4 with its lifetime of 19.6 hours (Figures 2b and 2c). The behavior of NO and N(^{4}S) at 40 N is shown in Figure 4 where the densities of these two species are plotted as a function of time for the three day period. On days 267 and 269, the density of N(^{4}S) atoms reach a maximum at 1300 hours UTC which is local solar noon. On these two days the density of NO is normal. On day 268, the NO increases reaching a maximum at 1300 hours UTC (local solar noon). The N(^{4}S) density has decreased because of the temperature-sensitive reaction of N(^{4}S) with O_2 (reaction 3). The lower N(^{4}S) density allowed the NO density to increase because of a decrease in the rate of reaction 2, the reaction of N(^{4}S) with NO. The role of N(^{4}S) in lowering the loss rate of nitric oxide was recognized by *Siskind et al.* [1989].

7. Comparison With Observations

[38] The results of the calculations with the TIEGCM model are compared with observations of nitric oxide density obtained with the SNOE satellite. The altitude region that is chosen for the comparison is 150 km. This is the highest altitude where SNOE NO measurements have satisfactory signal to noise ratio. This is also an altitude where Joule heating has a significant effect on the NO density. Since the SNOE satellite was in a sun-synchronous orbit at a local solar time of 1100 hours, each orbit is at a different longitude while the universal time increases by 1.6 hours for subsequent orbits. Table 1 lists the longitude and local time of the fifteen orbits for day 268.

[39] In Figure 5 (middle), SNOE measurements of nitric oxide density are plotted as a function of orbit and latitude for the three day period 267–269 in 1998 and for the latitude region 0–80°N. The observations were made at a local time of 11:00. The 15 orbits per day were spaced apart 24 degrees in longitude and 1.6 hours in Universal Time. In Figure 5 (top), the results of the TIEGCM calculations are plotted for the same time, altitude, latitude and longitude as the SNOE observations. The color scales of the SNOE and TIEGCM data are adjusted to show a full range of colors with red being the maximum and dark blue the minimum. The maximum SNOE NO density is 13 % greater than the maximum TIEGCM model NO density.

[40] A first comparison of Figures 5a and 5b shows that there are large increases in nitric oxide density in both the observations and the model as a result of the Joule heating event. In the middle of day 268 from 1000 to 1300 hours

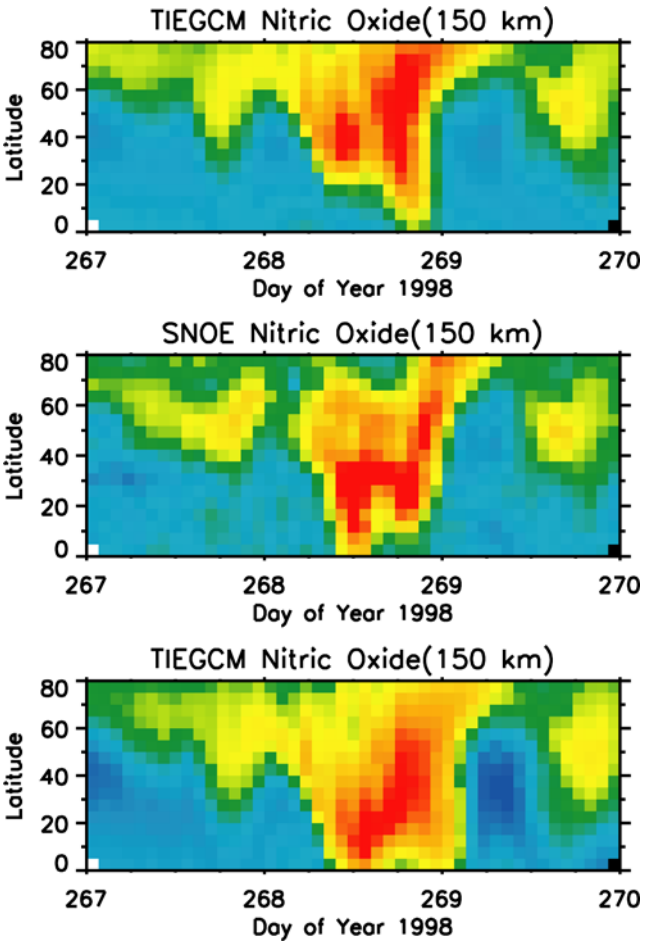

Figure 5. (top) TIEGCM nitric oxide density at 150 km as a function of time and latitude. The NO densities have been extracted from the TIEGCM results for the latitude, longitude, and time of the SNOE observations. The maximum of the color scale is 5.5 × 10^7 molecules/cm^3. (middle) SNOE nitric oxide density at 150 km for the 3-day period 267–269. Fifteen orbits of data are plotted. The maximum of the color scale (red) is 7.7 × 10^7 molecules/cm^3. (bottom) TIEGCM nitric oxide density at 150 km for model run with Joule heating doubled. The maximum of the color scale (red) is 8.0 × 10^7 molecules/cm^3.

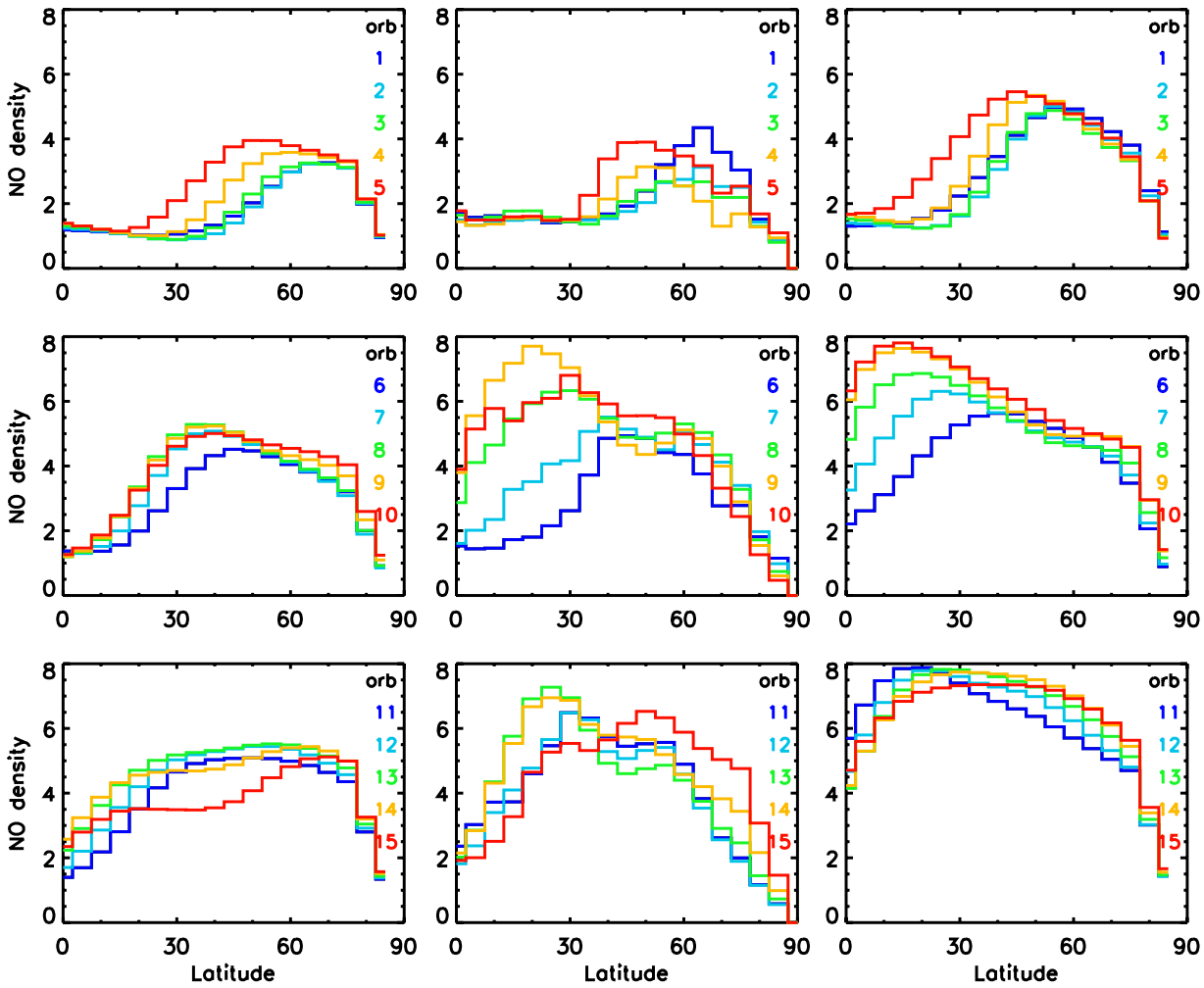

Figure 6. Comparison model and observations for fifteen orbits on day 268. The longitude and UT of the 15 orbits are listed in Table 1. TIEGCM nitric oxide densities (10^7molecules/cm^3) at 150 km are plotted in the left. SNOE nitric oxide observations are in the middle. TIEGCM nitric oxide densities (10^7molecules/cm^3) with Joule heating doubled are plotted in the right. The effect of Joule heating is shown in orbits 5–14. Both model and observations show increasing nitric oxide moving equatorward. The equatorward extent of the observations lies between the predictions of the two model runs.

UTC there is a large increase in nitric oxide density between 20°N and 40°N as a result of the Joule heating event. There is a second surge in the low-latitude nitric oxide between 1800 and 2100 hours UTC. Starting at 2200 hours on day 268, the nitric oxide density starts to decrease and retreat northward during the first six hours of day 269. Both the model and the observations show the low-latitude increase in nitric oxide that is the result of Joule heating at high latitudes. The observations show the nitric oxide density extending to lower latitudes than the model calculations do. To explore the model-observations comparison further, a second model calculation was performed by doubling the amount of Joule heating. The results of this second model calculation are shown in Figure 5 (bottom). In the middle of day 268 between 1000 and 1300 hours, the amount of nitric oxide has increased and moved further equatorward as compared to the results of the first model calculation. The maximum SNOE NO density is now 13% lower than the maximum NO density from the second TIEGCM calculation. The reasons for our doubling the magnitude of the Joule heating were twofold: to clearly demonstrate the effect of Joule heating on nitric oxide and to bracket the magnitude of the nitric oxide densities measured by SNOE.

[41] The results of the two model calculations and the SNOE observations are shown in Figure 6 in a series of latitude-density plots for the fifteen orbits of day 268. The plots on the left show the nitric oxide densities from the model calculation using the amount of Joule heating determined from the AMIE calculations. The plots in the center show the nitric oxide densities measured from the SNOE satellite. The plots on the right have the results of the second model calculation with double the amount of Joule heating. A comparison of the latitude distribution of nitric oxide in the plots shows that the observations lie between the two model calculations with the observations reaching a maximum density at a latitude of 20 N at 1300 hours UTC during orbit 9. A comparison between the two model calculations shows that doubling the amount of Joule heating increases

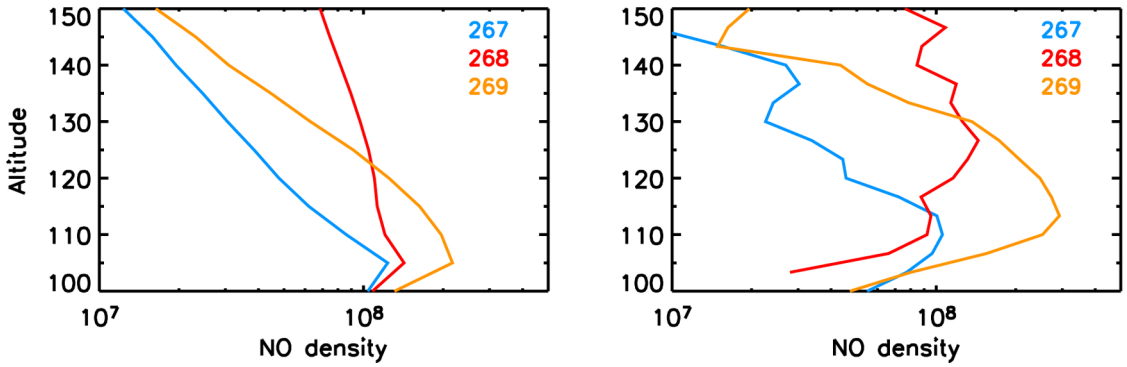

Figure 7. Nitric oxide densities as a function of altitude are shown for days 267, 268, and 269. The latitude is 30°N, and the longitude is 314°E. Day 267 (blue) is the day before the Joule heating event, day 268 (red) is the day of the event, and day 269 (orange) is day after the event. The TIEGCM simulations are shown in the left, and the SNOE observations are shown in the right.

the maximum nitric oxide density by 50% and moves the maximum equatorward from 35°N to 15°N. The comparison of the two model results demonstrates how Joule heating at high latitudes can affect nitric oxide density at low latitudes. The gravity wave generated by the Joule heating propagates equatorward heating the atmosphere by conduction [*Richmond*, 1978]. At low latitudes the photochemistry of the heated atmosphere produces the increase in the nitric oxide density. Doubling the amount of Joule heating in the second model calculation caused the gravity wave to propagate further equatorward and heat the atmosphere to a higher temperature.

[42] The comparison of SNOE observations and the TIEGCM model calculations at 150 km shows that the model reproduces the features that are present in the observations. During the Joule heating event, hours 0600–1300 UTC on day 268, the temperature of the atmosphere rapidly increases all the way to the equator. In response to the temperature change, the nitric oxide increases at all latitudes starting at 1200 hours and lasting to 2300 hours. The atmosphere then begins to cool and the nitric oxide density decreases to normal levels during the first six hours of day 269.

[43] All of the preceding description of the TIEGCM model and the SNOE observations has been for the 150 km altitude level. The SNOE database actually includes observations between 100 and 150 km. An examination of the altitude dependence of the nitric oxide density will tell us how Joule heating affects nitric oxide at lower altitudes. Figure 7 shows the altitude dependence of nitric oxide for three successive days at a latitude of 30°N and a longitude of 314°E. This latitude was chosen to show how Joule heating which occurs at high latitudes also heats the thermosphere at lower latitudes. The Joule heating event was at its maximum at 0600 hours UTC on day 268. The SNOE observations of longitude 314 E were made at 1300 hours UTC. In Figure 7 (right), there are three altitude profiles: the blue line corresponds to day 267 (the day before the Joule heating event), the red line is for day 268 (the day of the event), and the orange line is for day 269. The day 267 profile shows a normal nitric oxide density distribution. On day 268, there is a large increase in the nitric oxide density particularly at the higher altitudes. On day 269, the nitric oxide decreases at higher altitudes and increases at lower altitudes indicating that the nitric oxide is diffusing downward in the thermosphere. Figure 7 (left) shows altitude profiles calculated with the TIEGCM model that had doubled the amount of Joule heating for the same latitude, longitude, and time for the same three days. The model also shows a normal profile on day 267, a large increase at high altitude on day 268, and increase in nitric oxide density at 110 km on day 269 that is the result of downward diffusion.

[44] Both the model calculations and the observations in Figure 7 clearly show that Joule heating which occurs in the 55°–60°N latitude region is responsible for the increase in nitric oxide at mid latitudes (30°N) and that this increased nitric oxide density diffuses downward to the 110–120-km region of the thermosphere where it causes an increase in nitric oxide density which lasts for a day.

8. Summary

[45] This study on how Joule heating affects nitric oxide densities in the thermosphere has revealed a sequence of physical processes. The Joule heating event occurs at high latitudes in the 150 km altitude region and lasts for several hours. The temperature increases by several hundred degrees C and then slowly decreases over a 24 hour period. A southward blowing meridional wind is generated and last for an hour or two. Gravity waves propagate equatorward, heating the thermosphere through conduction all the way to 20°N in a period of one or two hours. When the heated thermosphere is illuminated by solar radiation, particularly the soft X rays, the density of nitric oxide at all latitudes increases and reaches a maximum at local noon. During the following 24 hours the increased nitric oxide diffuses downward from the 150-km region to 110 km.

[46] The increase in nitric oxide is initiated by the temperature-sensitive reaction between $N(^4S)$ atoms and molecular oxygen. However, it is still the reaction between $N(^2D)$ and molecular oxygen that produces the nitric oxide, but the density of nitric oxide increases because the loss rate of nitric oxide decreases due to the decrease in density of $N(^4S)$ atoms. After the Joule heating event, the density of nitric oxide returns to normal when the density of $N(^4S)$

atoms increases to its normal amount. During the Joule heating event there is upwelling at high latitudes that increases the density of molecular oxygen. This increased molecular oxygen density also causes the nitric oxide density to increase, but it is not the major cause.

[47] The answers to the two questions posed in the introduction are as follows:

[48] 1. the increase in nitric oxide density equatorward of the auroral region during a Joule heating event is the result of the transport of heat equatorward by a gravity wave with the increase in nitric oxide taking place at midlatitudes,

[49] 2. both the SNOE observations and the TIEGCM calculations show that the increase in nitric oxide density in the 150-km level is followed by downward transport of nitric oxide molecules to the 110-km level.

[50] This has been a study of an individual Joule heating event that occurred near equinox, but it is expected that this same sequence of atmospheric processes takes place for the many Joule heating events that occur throughout the year.

[51] **Acknowledgments.** National Center for Atmospheric Research (NCAR) is supported by National Science Foundation (NSF). Work at NCAR was partly supported by NASA Guest Investigators program. The publication of this paper has been supported by the NASA Resident Archive program.

[52] Zuyin Pu thanks the reviewers for their assistance in evaluating this paper.

References

Barth, C. A., and S. M. Bailey (2004), Comparison of a thermospheric photochemical model with Student Nitric Oxide Explorer (SNOE) observations of nitric oxide, *J. Geophys. Res.*, *109*, A03304, doi:10.1029/2003JA010227.

Barth, C. A., K. D. Mankoff, S. M. Bailey, and S. C. Solomon (2003), Global observations of nitric oxide in the thermosphere, *J. Geophys. Res.*, *108*(A1), 1027, doi:10.1029/2002JA009458.

Barth, C. A., D. N. Baker, and S. M. Bailey (2004), Seasonal variation of auroral electron precipitation, *Geophys. Res. Lett.*, *31*, L04809, doi:10.1029/2003GL018892.

Dobbin, A. L., and A. D. Aylward (2008), A three-dimensional modeling study of the processes leading to mid latitude nitric oxide increases in the lower thermosphere following periods of high geomagnetic activity, *J. Adv. Space Res.*, *42*, 1576–1585, doi:1016/j.asr.2008.03.004.

Lu, G., A. D. Richmond, B. A. Emery, and R. G. Roble (1995), Magnetosphere-ionosphere-thermosphere coupling: Effect of neutral winds on energy transfer and field-aligned current, *J. Geophys. Res.*, *100*(A10), 19,643–19,659.

Lu, G., A. D. Richmond, R. G. Roble, and B. A. Emery (2001), Coexistence of ionospheric positive and negative storm phases under northern winter conditions: A case study, *J. Geophys. Res.*, *106*(A11), 24,493–24,504.

Richards, P. G. (2004), On increases in nitric oxide density at mid latitudes during ionospheric storms, *J. Geophys. Res.*, *109*, A06304, doi:10.1029/2003JA010110.

Richmond, A. (1978), The nature of gravity wave ducting in the thermosphere, *J. Geophys. Res.*, *83*(A4), 1385–1389.

Richmond, A. D., and Y. Kamide (1988), Mapping electrodynamic features of the high-latitude ionosphere from localized observations: Technique, *J. Geophys. Res.*, *93*(A6), 5741–5759.

Richmond, A. D., E. C. Ridley, and R. G. Roble (1992), A thermosphere/ionosphere general circulation model with coupled electrodynamics, *Geophys. Res. Lett.*, *19*(6), 601–604.

Roble, R. G., and E. C. Ridley (1987), An auroral model for the NCAR thermospheric general circulation model (TGCM), *Ann. Geophys. Ser. A*, *5*, 369–382.

Roble, R. G., and E. C. Ridley (1994), A thermosphere-ionosphere-mesosphere-electrodynamics general circulation model (time-GCM): Equinox solar cycle minimum simulations (30–500 km), *Geophys. Res. Lett.*, *21*(6), 417–420.

Roble, R. G., E. C. Ridley, A. D. Richmond, and R. E. Dickinson (1988), A coupled thermosphere/ionosphere general circulation model, *Geophys. Res. Lett.*, *15*(12), 1325–1328.

Siskind, D. E., C. A. Barth, and R. G. Roble (1989), The response of thermospheric nitric oxide to an auroral storm: 1. Low and middle latitudes, *J. Geophys. Res.*, *94*(A12), 16,885–16,898.

Stevens, M. H. (1995), Nitric oxide gamma band fluorescent scattering and self-absorption: 1. The mesosphere and lower thermosphere, *J. Geophys. Res.*, *100*(A8), 14,735–14,742.

C. A. Barth, Laboratory for Atmospheric and Space Physics, University of Colorado, Campus Box 590, Boulder, CO 80309-0590, USA. (barth@lasp.colorado.edu)

G. Lu and R. G. Roble, High Altitude Observatory, National Center for Atmospheric Research, 3080 Center Green Drive, Boulder, CO 80301, USA.